Ground-based zenith sky abundances and *in situ* gas cross sections for ozone and nitrogen dioxide with the Earth Observing System Aura Ozone Monitoring Instrument

Marcel Dobber, Ruud Dirksen, Robert Voors, George H. Mount, and Pieternel Levelt

High-accuracy spectral-slit-function calibration measurements, *in situ* ambient absorption gas cell measurements for ozone and nitrogen dioxide, and ground-based zenith sky measurements with the Earth Observing System Aura Ozone Monitoring Instrument (OMI) flight instrument are reported and the results discussed. For use of high-spectral-resolution gas absorption cross sections from the literature in trace gas retrieval algorithms, accurate determination of the instrument's spectral slit function is essential. Ground-based measurements of the zenith sky provide a geophysical determination of atmospheric trace gas abundances. When compared with other measurements, they can be used to verify the performance of the OMI flight instrument. We show that the approach of using published high-resolution absolute absorption cross sections convolved with accurately calibrated spectral slit functions for OMI compares well with *in situ* gas absorption cell measurements made with the flight instrument and that use of these convolved cross sections works well for reduction of zenith sky data taken with the OMI flight instrument for ozone and nitrogen dioxide that are retrieved from measured spectra of the zenith sky with the differential optical absorption spectroscopy technique, the same method to be used for the generation of in-flight data products. Finally, it is demonstrated that the spectral stability and signal-to-noise ratio performance of the OMI flight instrument, as determined from preflight component and full instrument tests, are sufficient to meet OMI mission objectives.

OCIS codes: 010.1280, 120.0280, 280.1310, 300.6190.

1. Ozone Monitoring Instrument

A. Introduction to the Ozone Monitoring Instrument

The primary objective of the Ozone Monitoring Instrument (OMI) on the Earth Observing System (EOS) Aura satellite is to obtain high-spatial-resolution global measurements of a number of atmospheric trace gases in both the troposphere and the stratosphere, with emphasis on ozone and nitrogen dioxide. These measurements will address science questions concerning the recovery of the ozone layer, the depletion of ozone at the poles, tropospheric air pollution, and climate change.

The concentrations of the constituents will be retrieved by algorithms developed for the NASA total ozone mapping spectrometer (TOMS) instrument[1] and differential optical absorption spectroscopy[2,3] (DOAS) algorithms developed for OMI at the Royal Netherlands Meteorological Institute (KNMI). These algorithms use nadir observations of backscattered light from the Sun from the Earth's atmosphere and ground in the ultraviolet–visible (UV–VIS) spectral wavelength range (270–500 nm). Column measurements of ozone, nitrogen dioxide, and other trace gases will be made. The vertical distribution of ozone will be determined by a method that makes use of the rapid increase in the ozone absorption cross section toward shorter wavelengths (Hartley bands).[4,5] The retrieval methods used for instruments like the Global Ozone Monitoring Experiment (GOME), the Scanning Imaging Absorption Spectrometer for Atmospheric Cartography (SCIAMACHY), the TOMS,

M. Dobber (dobber@knmi.nl), R. Dirksen, R. Voors, and P. Levelt are with the Royal Netherlands Meteorological Institute, P.O. Box 201, 3730 AE De Bilt, The Netherlands. R. Dirksen is also with Space Research Organization Netherlands, Sorbonnelaan 2, 3584 CA Utrecht, The Netherlands. G. H. Mount is with the Department of Civil and Environmental Engineering, Washington State University, Pullman, Washington 99164-2910.

Received 20 January 2004; revised manuscript received 2 July 2004; accepted 23 December 2004.

0003-6935/05/142846-11$15.00/0

and the solar backscatter ultraviolet instrument will also be applied to OMI spectra.

To meet the science objectives, measurements are needed that combine good spatial resolution with daily global coverage. Since determination of tropospheric trace gas abundances for monitoring of air pollution (e.g., regional urban air pollution, biomass burning) requires cloud-free observations, high spatial resolution is required to optimize the probability of observing cloud-free conditions. Determining tropospheric pollution levels on a high spatial and regional scale is essential to study the human effect on the Earth's atmosphere and climate.

OMI will deliver spectral radiances and irradiances from 270 to 500 nm, and these will be used to retrieve the primary data products ozone total column, ozone vertical profile, UV-B flux, nitrogen dioxide total column, aerosol optical thickness, cloud effective cover and cloud top pressure, and secondary data products such as total column SO_2, BrO, HCHO, and OClO. Most of these products are obtained from direct spectroscopic observation. The cloud top pressure is obtained from interpretation of the Ring effect and $O_2 - O_2$ absorption.[6,7]

To retrieve trace gas abundances from the observed Earth reflectance spectrum, the DOAS technique fits the observed differential spectral absorption features with an accurate spectrum of the attenuation derived from the photoabsorption cross section of the trace gas, convolved to OMI spectral resolution. There are two ways in which the trace gas cross sections at instrument resolution can be obtained. First, they can be measured directly with the flight instrument and absorption gas cells at a number of different pressures and temperatures. Second, they can be determined by convolving published high-resolution calibrated cross-section measurements with the accurately measured instrument spectral slit function. Early in the OMI project the choice was made to perform an accurate calibration of the shape of the spectral slit function at all pertinent wavelengths and viewing directions rather than performing gas cell measurements at various pressures and temperatures.

The outline of this paper is as follows. First, the OMI is introduced and its design features are described. The spectral-slit-function measurements are described and discussed. Gas absorption cell measurements for ozone and nitrogen dioxide measured with the OMI flight instrument are discussed. The attenuations derived from high-resolution absorption cross-section spectra from the literature are convolved with the accurately measured OMI spectral slit functions and compared with these absorption gas cell measurements to investigate whether they yield the same results. These measurements validate the general approach we envision for DOAS retrievals selected for the OMI project: Namely, use of attenuations derived from high-resolution absorption cross-section data from the literature convolved with the accurately calibrated spectral-slit-function response. The OMI is the first instrument of its type that uses this approach for the retrieval of the Earth atmospheric constituents in flight. This is followed by a discussion of the ground-based zenith sky measurements of the real atmosphere to derive abundances of atmospheric trace gases with the flight instrument. From the zenith sky analysis it is shown that the OMI is capable of measuring the atmospheric ozone and nitrogen dioxide with the expected accuracies.

B. Ozone Monitoring Instrument Description

The OMI is a compact nadir-viewing UV–VIS imaging spectrograph with two spectral channels each having a two-dimensional frame transfer CCD detector. The large 114° field of view (FOV) perpendicular to the flight direction yields a 2600-km-wide spatial swath large enough to achieve global daily coverage of the Earth's atmosphere at the equator. The in-flight net integration time of 2 s, consisting of coadded 0.4-s individual exposures, sets the spatial sampling in the flight direction to 13 km. The CCD detector has a frame transfer layout to allow simultaneous exposure and readout of the previous exposure, avoiding data loss during readout. The dimensions of the CCD detectors are 814 (wavelength dimension) by 578 (viewing dimension) pixels. In the nominal operational mode (global mode) eight CCD rows are electronically added (binned) in the viewing dimension during the readout, so spectra from neighboring viewing directions are summed. This decreases the contribution of the readout noise and the internal data rate, increases the signal-to-noise ratio, and reduces the sampling in the swath dimension to 60 binned pixel rows (30 for wavelengths below 310 nm). Binning sets the ground pixel size in the swath direction to 24 km (48 km for wavelengths below 310 nm). The size of a binned pixel projected on the Earth's surface is 13 km $\times$ 24 km (flight direction $\times$ swath direction) in the nadir direction (13 km $\times$ 48 km for wavelengths below 310 nm). This small ground pixel size and the simultaneous availability of the complete swath are significant improvements over other recent instruments such as GOME and SCIAMACHY and increase the chance of observing cloud-free pixels, necessary for determination of tropospheric trace gas concentrations. With a two-dimensional CCD, the spectrum of every ground pixel is recorded simultaneously preventing the spatial aliasing, i.e., different ground pixels are observed at different times, which results from use of a scan mirror. The spectrum is registered in one dimension of the CCD, and the spatial FOV is recorded in the other dimension.

The layout of the OMI optical bench depicting the telescope and the UV spectral channel is presented in Fig. 1; the large spatial swath is out of the plane of the paper. The telescope consists of a primary mirror, a polarization scrambler, and a secondary mirror that focuses the incident radiance on the spectrograph entrance slit. Solar irradiance enters the instrument through the solar port, which has a 10% transmission mesh, to illuminate a reflection diffuser. A folding mirror reflects the diffuser signal into the main opti-

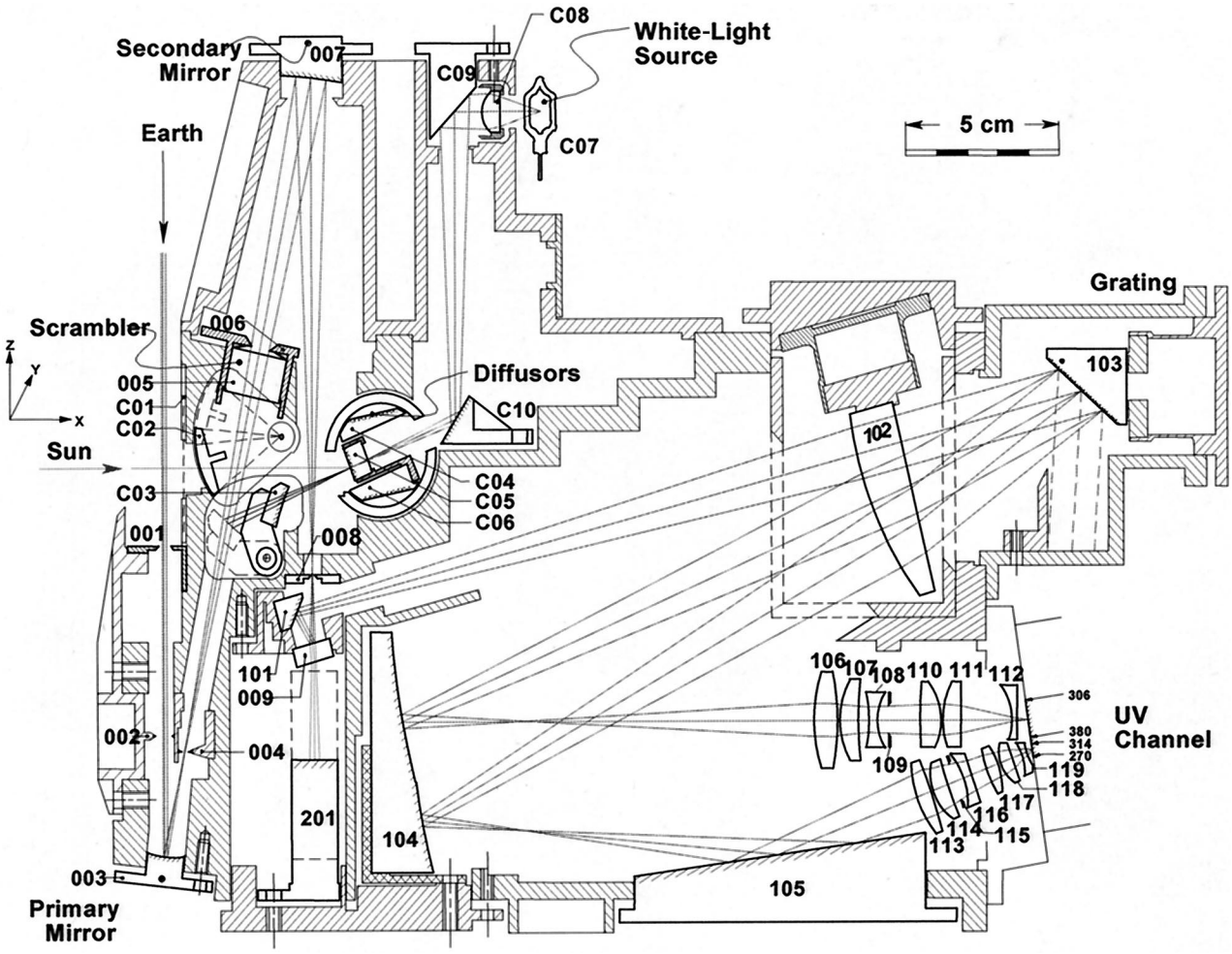

Fig. 1. Layout of the optical bench of the OMI. Telescope plus UV spectral channel.

cal path just before the polarization scrambler. The polarization scrambler makes the instrument insensitive to the polarization state of the reflected Earth radiance to less than 0.5%. An onboard white-light source for in-flight spectrograph testing is coupled through a transmission diffuser and the solar folding mirror. This optical path was also used during the on-ground calibration to mount an external optical stimulus close to the internal white-light source. The beam entering the spectrograph from either of the onboard diffusers illuminates the full length of the spectrograph slit and thereby all spatial viewing directions (CCD rows) within the FOV. In the spectrograph the beam is split into two channels: UV (270–380 nm) and VIS (350–500 nm). The UV channel is separated into two subchannels: UV1 (270–310 nm) and UV2 (300–380 nm) by the two-part mirror labeled 104. Mirror 104 is segmented and has a spatially grading efficiency coating that reduces reflectance of higher wavelengths at the lower part of the mirror to reduce stray light at the low wavelengths (below 310 nm). The UV1 channel is spatially scaled down by a factor of 2 in both dimensions relative to the UV2 subchannel to improve the signal-to-noise ratio. Spectral dispersion in the focal plane is 0.32, 0.15, and 0.21 nm for UV1, UV2, and VIS, respectively, per 22.5-μm detector pixel. The ratio between the spectral resolution and the imaged slit size in the focal plane (width of a spectral feature) is $\sim$3 in UV2 and VIS to avoid any difficulties caused by aliasing in the process of trace gas retrieval. The spatial and spectral properties of the OMI are summarized in Table 1.

An extensive on-ground calibration program was performed with the purpose to determine the radiometric calibration parameters with 1% (1σ) accuracy for the absolute radiance and irradiance calibrations (without the error contribution from the used radiative standards) and 1% (1σ) for the irradiance mode bidirectional scattering distribution function. It is important to verify and maintain an accurate calibration of the instrument in flight. The in-flight calibration of the OMI is accomplished with

(1) A set of three reflective diffusers for absolute radiometric calibration by daily measurement of the Sun. Two of the three diffusers are conventional ground aluminum diffusers, one to be used on a weekly basis, the other to be illuminated monthly to monitor the degradation of the first diffuser. The deg-

Table 1. Spectral and Spatial Properties for the Channels of the OMI Instrument

Channel	Wavelength Range (nm)	Sampling (nm/pixel)	Resolution (nm)	Pixel Size (Binning 8)	Number of Rows in Swath Dimension
UV1	270–310	0.32	0.65	13 km × 48 km	30
UV2	305–375	0.15	0.45	13 km × 24 km	60
VIS	350–500	0.21	0.65	13 km × 24 km	60

radation is expected to be a function of the integrated sunlight exposure time as evidenced by other satellite instruments (e.g., TOMS[1]). The third diffuser is a double ground quartz volume diffuser that is to be used on a daily basis. The term volume diffuser refers to the fact that the first ground surface is used as a transmission diffuser, and the second aluminum-coated surface acts as a reflectance diffuser. The first surface finally acts as a third transmission diffuser. The thickness of the diffuser is ~6 mm. These multiple diffusive surfaces reduce the effect of surface structures. The volume diffuser was implemented on OMI since ground aluminum diffusers exhibit wavelength-dependent structures that affect the accuracy of the radiometric calibration and that interfere with the DOAS retrieval of data products. As a result of its smooth surface and the multiple diffusive surfaces, the spectral structures introduced by the volume diffuser are at least an order of magnitude smaller. The diffusers are well protected from contamination and solar light while not in use.

(2) The white-light source provides relative radiometric calibration and information about the degradation of the detector (bad and dead pixels).

(3) Two LEDs per subchannel (UV1, UV2, VIS) mounted in the proximity of the detector are also used to trace bad and dead pixels.

(4) During the eclipse side of the Earth orbit, the dark signal will be calibrated by performing both long-exposure-time dark measurements and dark signal measurements with instrument settings identical to radiance measurements at the dayside of the orbit.

(5) Spectral calibration will be performed by use of Fraunhofer lines in solar and Earth nadir spectra. Since the OMI spectral slit function is known with high accuracy from the on-ground calibration, a wavelength calibration with an accuracy of 0.01 detector pixel is obtained by use of a high-resolution solar spectrum[8] and the observed in-flight spectra.

OMI has been developed by Dutch and Finnish industry under contract with the Netherlands Agency for Aerospace Programmes and the Finnish Meteorological Institute. The Royal Netherlands Meteorological Institute (KNMI) is the principal investigator institute for the OMI. An international OMI science team has approximately 60 members. The instrument was successfully launched on 15 July 2004 on NASA's EOS Aura satellite that flies in a polar Sun-synchronous orbit at approximately 700-km altitude. More details on the OMI design can be found elsewhere.[9–12]

2. Spectral-Slit-Function Measurements and Results

A. Spectral-Slit-Function Setup and Measurements

The calibration of the spectral properties of the OMI comprises two aspects: the wavelength assignment to each pixel of the two-dimensional detector array and the shape of the spectral response function (slit function) of each detector pixel. Both calibration parameters were measured with the OMI under flight-representative conditions. The slit function determines the measured spectral width (resolution) of the radiances (irradiances) spectral structures. Since the slit function is different for every detector pixel, its determination is of critical importance for DOAS-based retrieval of data products for which shapes must be accurately determined.

For the purpose of accurately measuring the slit function shape, a dedicated optical stimulus was designed that utilizes an echelle grating to produce an output beam containing ~50 tunable, well-separated, extremely narrow spectral peaks (corresponding to the large number of diffraction orders). By rotating the echelle grating, the spectral peaks move in wavelength space and thus on the OMI CCD detector. The response of a detector pixel to a passing echelle peak constitutes the spectral slit function of that pixel. Rotation of the echelle grating gives the shape of the spectral slit function, which is measured with better sampling and at higher accuracy than is obtained by use of a spectral line source, for which the accuracy is limited by the pixel sampling of the spectral resolution by the detector. As listed in Table 1, the ratio of the OMI spectral resolution to the pixel sampling is typically 3; in the dedicated slit function measurements with the echelle system, ten times better sampling of the spectral resolution is achieved. For the OMI the spectral slit function depends on wavelength (i.e., pixel), viewing direction (i.e., swath), and the temperature of the optical bench, which is fixed in flight at 265 K. The light beam of the echelle stimulus was coupled into the OMI by the calibration port (C08–C10 in Fig. 1), with the full length of the spectrograph slit and thereby all CCD rows (viewing angles) illuminated and thus enabling the slit function profile of all CCD pixels to be measured in a single measurement run (rotation of the echelle grating). During the performance test period, slit function measurements were performed illuminating the instrument through the nadir port, the Sun port, and the calibration port. It was verified that the slit function measured through all these illumination ports is

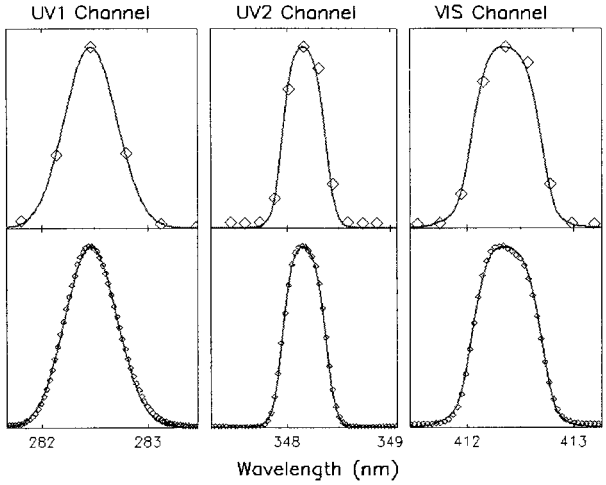

Fig. 2. OMI spectral-slit-function profile for each spectral channel. The upper panels present the OMI response to a single narrow wavelength corresponding to a single echelle angle measurement (or spectral line source) and clearly show the limited sampling of the spectral resolution of the instrument when illuminated with a spectral line. The lower panels present the OMI slit function calibrated with the dedicated optical stimulus at multiple echelle angles; much better sampling is achieved with this stimulus, which moves the spectral feature in pixel space as the echelle grating is rotated. The solid curves are a parameterized fit through the data: a Gaussian profile in UV1, a modified (broadened) Gaussian profile in UV2 and VIS. The fit result of the lower panels is coplotted in the upper panels to guide the eye.

identical. This is important for OMI-type instruments because Earth radiance spectra are divided by Sun irradiance spectra entering the instrument through different optical ports to obtain absolutely calibrated Earth reflectance spectra, which are the basis of all subsequent retrieval techniques. Because the spectral slit function is the same for all instrument entrance ports, no additional systematic noise will be added to these reflectances that results from imperfect cancellation of solar Fraunhofer structures in the radiance and irradiance spectra that originates from differing spectral-slit-function responses for the two measurement modes.

The initial wavelength calibration was performed with a hollow cathode PtCrNe spectral line source. As this line source lacks sufficiently strong lines in the long wavelength end of the OMI wavelength range, these measurements were combined with the slit function measurement data to derive the wavelength calibration, yielding an on-ground wavelength calibration accuracy of 1/10 pixel (~0.01 nm). This is sufficiently accurate for the analysis of the other on-ground calibration measurement data. The required accuracy for the in-flight wavelength calibration, 1/100 pixel, will be obtained with the Fraunhofer structures in the solar spectrum, which will be measured once per day.

B. Spectral-Slit-Function Results

The upper plots in Fig. 2 show the sampling of the spectral slit function when recording the response to the echelle slit function optical stimulus at a single echelle angle, and the lower plots show the improved sampling of the slit function measured with the dedicated echelle optical stimulus at multiple echelle angles. The solid curves in the top plots are a parameterized fit through the data points of the lower plots. Note that the solid curves in the upper plots are not a fit through the small number of data points. For the UV1 spectral channel, a standard Gaussian line shape was fitted; for the UV2 and VIS spectral channels, a modified, broadened Gaussian profile was used. The functional parameterization describing the broadened Gaussian profile is

$$A_0 \exp\left[-\left(\frac{x-x_0}{w_0}\right)^2\right] + A_1 \exp\left[-\left(\frac{x-x_1}{w_1}\right)^4\right], \quad (1)$$

where A_0, A_1, x_0, x_1, w_0, w_1 are the fitting parameters. Note that x_0 and x_1 can be different, resulting in asymmetric slit function shapes. The quality of the parameterization in the lower plots of Fig. 2 is quite good, but possibilities for improvement are being investigated by use of different parameterizations, especially in the wings of the profile.

The results show that, by use of the echelle grating optical stimulus, much more accurate calibration parameters for the spectral slit function can be obtained as compared with use of single spectral lines.

3. Results of Gas Absorption Cell Measurements of Ozone and Nitrogen Dioxide

Absorption gas cell measurements were performed with the OMI flight instrument on ozone and nitrogen dioxide at ambient temperature and pressure. The goal of these measurements is to show that the absorption spectra measured with the OMI are the same, within the applicable uncertainties, to the absorption spectra derived from the convolution of the published absorption cross sections and the accurately calibrated spectral slit functions. The OMI follows the heritage of the GOME and SCIAMACHY hyperspectral Earth observation instruments. Preflight characterization of the instrument response to a number of absorption gases, including ozone and nitrogen dioxide, under well-defined conditions has been carried out for these instruments with a dedicated measurement setup.[13–15] For the OMI gas absorption cell measurements a collimated beam of white light from a 300-W xenon high-pressure arc discharge lamp was passed through a 50.0-cm-long quartz single-pass gas cell 50 mm in diameter. The transmission of the cell windows is better than 90% at 270 nm and increases to longer wavelengths. The light is coupled into the instrument through the OMI calibration port, thus illuminating all viewing angles homogeneously. Special attention was given to make the illumination beam pass through the cell toward the instrument as homogeneously as possible. Homogeneous filling of the entrance slit of the instrument is important because inhomogeneous filling would lead to distorted spectral slit functions, thus compro-

mising the goals of the experiment. The gas cell was continuously flushed during measurements with premixed 200-parts per million by volume NO_2 in dry air from a gas bottle. This concentration was carefully selected to give absorbances of 5%–10% for the 50.0-cm cell length to ensure enough absorption for a good signal-to-noise ratio, but not enough absorption to push the regime into the nonlinear absorption region. Ozone was produced on site from an electrical discharge ozonizer (Innovatec CMG 3-3). The ozonizer was used with 99.998% pure oxygen at a 30 l/h flow rate to avoid formation of chemical by-products that could absorb in the OMI spectral region. Ozone concentrations of approximately 4×10^{16}, 8×10^{16}, 2×10^{17}, 4×10^{17}, and 8×10^{17} cm^{-3} were used. The exact concentrations are not known, but this is not crucial for the experiment since normalization to a well-determined literature value can be obtained after the fact. The main interest of the experiment was to measure the shape of the spectral features. After passing through the cell, the ozone was catalytically converted into molecular oxygen and fed into the gas exhaust system of the clean room. Since the measurements were done with the gas cell at ambient temperature and pressure, the room-temperature absorption spectrum was measured, although the OMI resided at stable thermal vacuum conditions (pressure $<10^{-5}$ hPa, optical bench temperature 265 K). Measurements were performed with the cell flushed with nitrogen dioxide or ozone and with an empty cell.

For the analysis of the cross section, the logarithm of the ratio of the flushed to empty cell OMI measurement is compared with the convolved literature cross section:

$$\sigma_{\mathrm{OMI}} \propto \ln(I^{\mathrm{OMI}}/I_0^{\mathrm{OMI}}) \text{ versus } \sigma_{\mathrm{LIT}}^{*}$$

$$= \ln[S \otimes \exp(\sigma_{\mathrm{LIT}})] \propto \ln\left[S \otimes \left(\frac{I}{I_0}\right)^{\mathrm{LIT}}\right], \qquad (2)$$

where I_0^{OMI} is the empty cell intensity, I^{OMI} is the flushed cell intensity, S is the OMI spectral slit function, and σ_{LIT} is the literature high-resolution absorption cross section. In the ratio of flushed/empty cell measurements, instrument and light source effects cancel resulting in a residual spectrum solely containing the NO_2 or ozone absorption spectrum as measured by the OMI.

The literature cross-section data used in this analysis are from Harder *et al.*,[16] which have an absolute accuracy of ±3% and a wavelength accuracy of one part in 10^7. The upper panel of Fig. 3 shows the convolved high-resolution literature NO_2 cross section between 420 and 450 nm overplotted with the scaled measurement with the OMI flight model. Results are given for the nadir-viewing angle. Even without scaling, the agreement is good. On the basis of the measurement setup parameters, the absolute cross section of NO_2 can be calculated from these OMI gas cell measurements. The NO_2 mixing ratio was

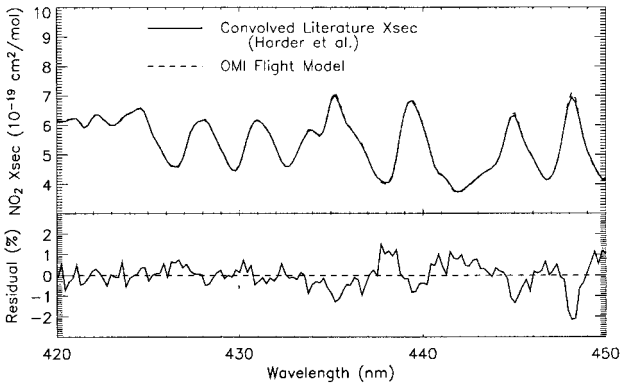

Fig. 3. Comparison between the room-temperature NO_2 absorption cross sections (x sec) measured directly with the OMI and derived from the high-resolution literature cross-section spectrum convolved with the measured OMI spectral slit function for the central viewing direction. The upper panel shows both results, the lower panel shows the residuals. The residuals have a rms value of ≈0.4%, indicating that the approach of accurately calibrated slit functions used for the data retrieval will work well.

200 ± 4 parts per million by volume and the gas cell was 50.0 ± 0.1 cm long, at ambient pressure and temperature. Under these conditions, the air density is 1.2 kg/m^3, which translates to 2.6×10^{19} molecules/cm^3 or 4.9×10^{15} NO_2 molecules/cm^3. For the 50.0-cm tube this yields a NO_2 particle density of 2.47×10^{17} molecules/cm^2. Use of this number in Beer's law then gives the absolute cross section. Given the fact that the gas cell measurements with OMI were not made to derive accurate absolute cross sections, and given the quoted uncertainty in the absolute values of the Harder *et al.* data of 3%, the agreement is excellent. The absolute NO_2 cross section derived from the OMI measurements has an almost constant difference with the convolved literature values of ~1%. The derived OMI cross sections (Fig. 3–6) were all corrected for this nearly constant difference by adding a second-order polynomial to the OMI-derived cross sections.

The lower panel of Fig. 3 shows the residual between the two curves in the upper panel. Most of the residual structure is noise (this is checked by making the same plots for adjacent rows), although some structure remains as well. There are a few possible reasons for this structure in the residual. Small changes in the wavelength calibration have a large effect on the residual. A shift of 0.03 nm causes a doubling of the rms error. The on-ground wavelength calibration is accurate to ≈0.1 pixel. In the VIS channel, this is ≈0.02 nm, so this is a likely source of error. Another possible reason, resulting from the spectral structure in the xenon lamp,[17] is expected to be small. This is inferred from measurements with a halogen light source, which is nearly flat in the wavelength region under investigation. Although the signal-to-noise ratio from these measurements was less than for the xenon lamp measurements, the halogen light source measurements show the same residues as for the xenon lamp within the accuracy of the

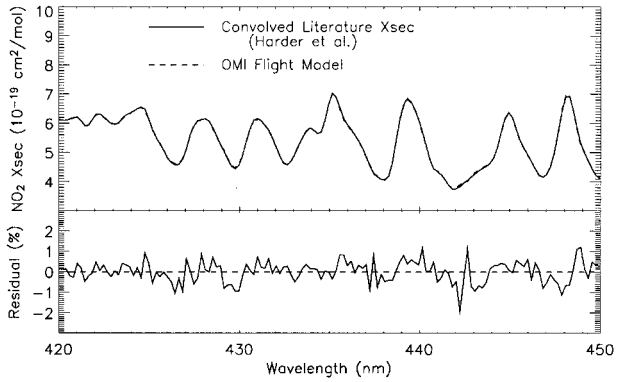

Fig. 4. Same as Fig. 3, but for a viewing direction of +35 deg.

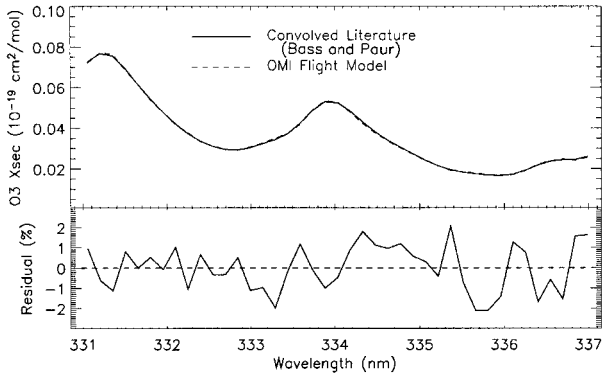

Fig. 6. Same as Fig. 5, but for the wavelength range 331–337 nm for the central viewing direction.

signal-to-noise ratio of the halogen lamp measurements.

The OMI slit functions have been accurately measured, so the effect of imperfect spectral-slit-function descriptions is expected to be small, but not entirely negligible. It is expected that with a more accurate slit function description the residues can still be decreased further. This research will be continued in flight when the real measurement data become available. The small residues indicate that the approach followed in the OMI project to use well-calibrated slit functions together with accurate high-resolution literature absorption cross-section spectra in the DOAS retrieval of trace gases will work well.

The spectral slit functions were accurately determined for each CCD detector pixel, i.e., for each viewing direction and wavelength. Figure 3 shows the result for NO_2 for the central viewing direction, but this result is representative for all viewing directions in the range −55 to +55 deg. This is exemplified in Fig. 4, which shows the result for NO_2 for the viewing direction of +35 deg. Comparisons for all viewing directions are similar to Figs. 3 and 4.

Figures 5 and 6 are the same as Fig. 3, but now for O_3 for the central viewing direction. For O_3 we show two separate graphs for two different reasons. First, the absolute cross section changes by almost 2 orders of magnitude in the UV2 channel.[18] Second, two different measurements were used to make the graphs. At short wavelengths, around 315 nm, the absorption resulting from ozone is very strong, so to obtain the best possible signal-to-noise ratio, we use a measurement with a relatively low ozone concentration in the gas cell (Fig. 5). At a longer wavelength, around 315 nm, the absorption is much weaker, so we used a measurement with a higher ozone concentration in the cell (Fig. 6). In both cases we find a rms error of ~0.5%. This is higher than expected from noise (~0.2% for these measurements) and is again tentatively attributed to an imperfect wavelength calibration. A similar check as for NO_2 on the gas particle density based on the measurement setup parameters shows larger differences between calculated and fitted quantities. Differences in absolute cross sections (see discussion on NO_2) for ozone were of the order of 10%. This is mainly due to the fact that the ozone concentration is derived from the voltage setting on the ozonizer. However, the relation between the voltage setting and the actual ozone concentration is not well known because these measurements were not performed to derive the absolute cross sections.

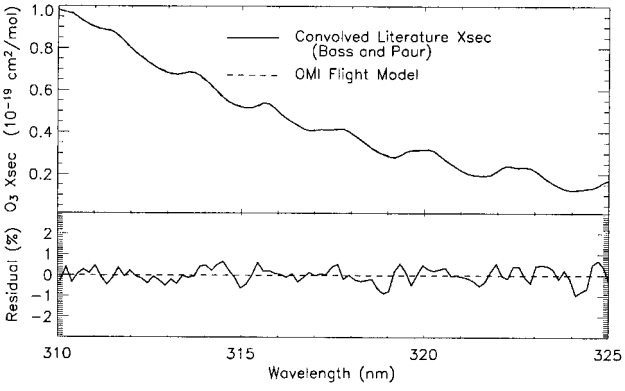

Fig. 5. Comparison between the room-temperature ozone absorption cross sections (x sec) measured directly with the OMI and derived from the high-resolution literature cross-section spectrum[18] convolved with the measured OMI spectral slit function for the central viewing direction in the wavelength range 310–325 nm. The upper panel shows both results, and the lower panel shows the residuals.

4. Zenith Sky Measurements and Results

During the preflight calibration period of the OMI, zenith sky measurements were performed with the instrument at flight-representative thermal vacuum temperature and pressure environmental conditions (pressure $<10^{-5}$ hPa, optical bench temperature 265 K). The goal of the zenith sky measurements was to check spectral stability and to demonstrate the ability to retrieve ozone and nitrogen dioxide column densities from the real atmosphere. The measurements were performed in Delft, The Netherlands (latitude 51.98° north, longitude 4.38° east), on 16 and 17 August 2002.

Zenith sky light entered through 30-cm holes cut in the roof and the clean room and was directed toward the instrument by three aluminum mirrors. The nadir port of the instrument was illuminated (no dif-

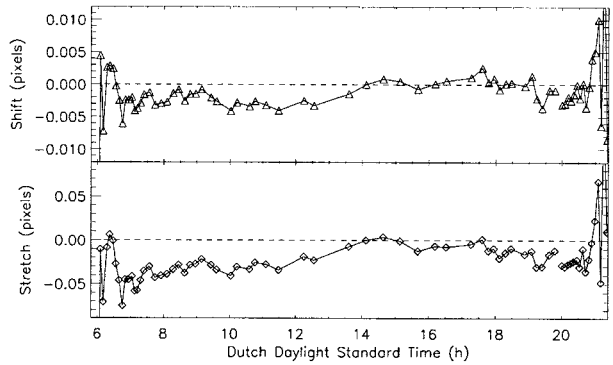

Fig. 7. In the upper panel the wavelength shift relative to the spectrum for a minimum SZA of 38° for the day is shown versus time for the VIS channel. In the lower panel the wavelength stretch across the entire CCD detector relative to the same spectrum is shown, also for the VIS channel.

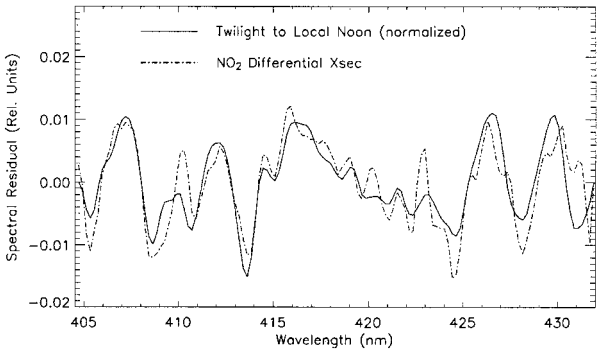

Fig. 8. Twilight OMI zenith sky data from 17 August 2002 at a SZA of 90° (solid curve) and desloped OMI NO_2 cross section (dotted–dashed curve). Even for these low signals a good fit is obtained. x sec, cross section.

fuser). The magnification of the telescope system with the curved aluminum mirror is ≈3, yielding a FOV of ≈2–3°. The 1° OMI FOV in the flight direction is thus filled completely and homogeneously. In the swath direction the FOV filling results in ≈14 rows on the CCD illuminated for the UV2 and VIS channels. Homogeneous filling of the entrance slit of the instrument is important to avoid distorted spectral slit functions that would compromise the goals of the experiment. In the analyses described below, 11 rows were averaged to increase the signal-to-noise ratio.

The weather conditions on both days were warm and sunny with a predominantly bright sky. The measurements started before sunrise during twilight conditions and lasted until after sunset, covering solar zenith angles (SZAs) between 36° and 95°. The wavelength scale throughout the day was monitored with respect to the local noon spectrum. The change in this scale was characterized by two parameters: a shift and a stretch (i.e., differential shift). Analysis of the individual measurements showed that shift and stretch of the spectrum relative to the spectrum taken at local noon was very small throughout the day, with the shift of the order of 0.004 detector pixel and the stretch less than 0.04 detector pixel over the entire wavelength range. Thus the spectral stability of the OMI is very good. Figure 7 shows the wavelength shift and stretch resulting from the DOAS analysis for the VIS channel relative to the minimum SZA spectrum. For this analysis the average, the slope, a fourth-order term (to mimic Rayleigh scattering), Ring effect,[6,7,19] and NO_2 absorption cell data as measured with OMI were included in the analysis.

The zenith sky data were analyzed for nitrogen dioxide and ozone. The measured signal-to-noise ratio for individual images around noon for a single detector row is ≈600. For the average over 11 rows the signal-to-noise ratio is measured to be ≈1750, as expected from instrument performance tests. Between 50 and 300 images were averaged for the analysis (6-s total integration time). The signal-to-noise ratio for an averaged image is ≈10,000, which is approximately a factor of 3 below what is expected from pure Poisson statistics. All spectra were ratioed with respect to the measurement taken at local solar noon, for which the optical path length through the atmosphere (air-mass factor) prior to being scattered into the instrument is the smallest. This technique was pioneered by Noxon in the mid-1970s and has become a standard technique for collecting detailed information about the atmosphere.[20–23]

Included in the molecular abundance analysis are spectral average, a slopelike term, a fourth-order term (to mimic Rayleigh scattering), and a Ring effect. The remaining structures in the resulting residual spectra are attributed to absorption by atmospheric trace gases and show up because of the large air-mass factor for these measurements near twilight. The Chappuis ozone, which interferes with the nitrogen dioxide bands to a minor extent, was not removed. Small effects in the residual spectrum are expected since a room-temperature cross section was used, whereas the stratospheric temperature is much colder.

An example of a twilight spectrum (high SZA angle) with a very low signal is shown in Fig. 8. The NO_2 absorption cross section is also shown in Fig. 8 to allow comparison with the structures observed in the measurement data. The purpose of Fig. 8 is to show that NO_2 can be observed directly in the measurement data. The shown NO_2 absorption cross section is thus not the result of a fit to the measurement data. A perfect match is not expected because of the presence of other absorbers in the atmosphere. Even for these spectra with very low signals, the NO_2 is clearly visible and the data can be fitted accurately. After subsequent removal of the fitted trace gas spectrum from the previous steps, in this case ozone and nitrogen dioxide, no systematic features (e.g., a wavelike structure from an instrument artifact) that could indicate a problem or instability in the data or the instrument are visible.

Performing a DOAS fit on the spectrum yields a relative slant column density (relative to the local solar noon measurement). Figure 9 shows the relative NO_2 slant column density that was retrieved

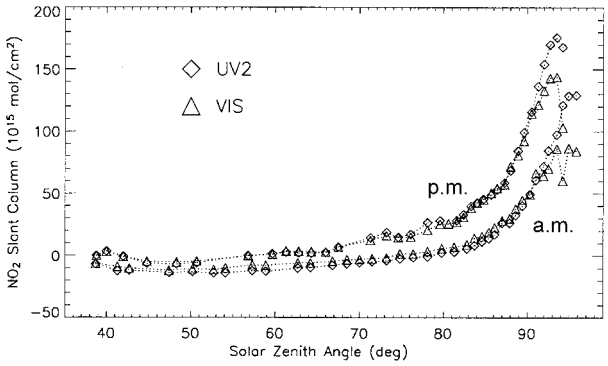

Fig. 9. Plot of the NO_2 slant column densities relative to local noon versus the SZA derived from the 17 August 2002 zenith sky measurements with the OMI. The NO_2 slant columns retrieved from the UV2 (diamonds) and the VIS (triangles) spectral channel agree very well.

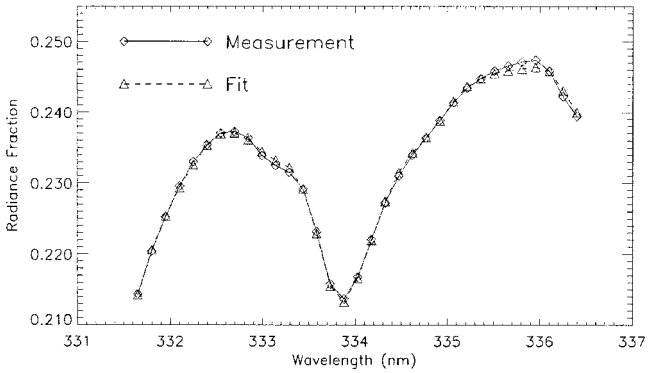

Fig. 10. Example of a DOAS fit to the wavelength window used for the retrieval of the total ozone column. The solid curve is the measurement, and the dashed curve is the fit.

from the zenith sky data for 17 August as a function of the SZA. We performed the DOAS retrieval on data from the UV2 and VIS channels using 345–373- and 403–432-nm fitting windows, respectively. Fits were performed with the attenuation derived from the literature absorption cross-section spectrum of NO_2 convolved with the accurately calibrated spectral slit function. The curves are not exactly smooth, as expected from the occurrence in Delft of local air pollution episodes, and the relative slant column densities rapidly increase for large SZAs in accordance with the rapidly increasing air-mass factors for these geometries. The a.m. curve is lower than the p.m. curve as expected from the formation of N_2O_5 at night and its subsequent temperature-dependent photodissociation during the day. Column NO_2 is expected to be less in the morning than in the afternoon. There is good compliance between the results obtained from the UV2 (fitting window 345–373-nm) and from the VIS (fitting window 403–432-nm) channels. In flight a fit window of 405–465 nm will be used for NO_2. The differences between the results for the UV2 and VIS channels are mainly attributable to the wavelength dependence of the air-mass factor, which is different at shorter wavelengths than at longer wavelengths, especially when boundary layer air pollution is of significance.

DOAS fits were also made to the UV2 data (331.6–336.6 nm) to retrieve ozone. This fit wavelength window is the same window that will be used in flight to retrieve total column ozone. The results of these fits are shown in Figs. 10 and 11. In Fig. 10 the measured response in the ozone retrieval window is shown along with the attenuation derived from the literature cross-section data from Bass and Paur,[18] convolved with the measured spectral slit function. The agreement between the two is good. The fit in Fig. 10 includes ozone at a temperature of 220 K and a Ring effect. The measured response in Fig. 10 is the fraction of two zenith sky measurements, one taken at 6 a.m. (SZA of 80.21 deg) and the other at 6.43 p.m. (SZA of 86.68 deg). Any fraction of two zenith sky measurements that day with a reasonable difference in slant column gives similar results.

Figure 11 shows the relative ozone slant column as a function of the cosine of the SZA. The a.m. and p.m. data nicely fall on top of each other, suggesting that the total ozone column did not change significantly during the day. From the slope of the curve for SZAs less than 60 deg, a rough estimate of 340 Dobson units (DU) is obtained. This value is in reasonable agreement with the result of 314 DU obtained with the KNMI Brewer spectrometer on the same day in De Bilt, The Netherlands, some 60 km to the east of Delft, and with the result of 313 $\pm$ 4 DU obtained from measurements with the GOME satellite instrument for that day. These results show that for ozone the approach for DOAS in which we use published absorption cross-section data and accurately calibrated spectral slit functions works well and that the OMI in space is capable of retrieving ozone from the Earth radiance measurement data.

The results of the zenith sky measurements show that ozone and nitrogen dioxide can be retrieved accurately from OMI measurement data by use of the DOAS technique and published laboratory absorption cross-section data and accurately measured spectral slit functions. The required signal-to-noise ratio

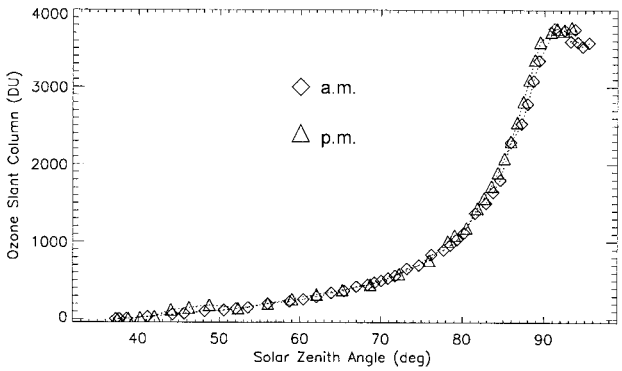

Fig. 11. Retrieved relative ozone slant column as a function of the cosine of the SZA. The fact that the a.m. and p.m. data fall on top of each other suggests that the vertical ozone column has not changed significantly during the day.

values for OMI in flight are 2600 for NO_2 total vertical columns for the global mode (13 km × 24 km) and 265 for the total ozone vertical columns. The other atmospheric constituents have signal-to-noise ratio required values that lie in between these values for NO_2 and ozone. These signal-to-noise ratio values allow for retrieval accuracies of 2% (~4 DU) for the total vertical ozone column and 10% for the total vertical NO_2 column in unpolluted cases (20% for a polluted case with tropospheric NO_2). In our analyses of the zenith sky measurement data we used binning factors, exposure times, and a number of averaged images to simulate as closely as possible the signal-to-noise ratios that are expected for typical in-flight light flux levels. In doing so we have taken into account the fact that in flight the Earth data will be referenced to a daily solar measurement by the volume diffuser, which will have a signal-to-noise ratio of ≈10,000, whereas on ground we used the local noon spectrum (average of 50 images) as a reference, which has approximately the same signal-to-noise ratio.

On the basis of the results for ozone and nitrogen dioxide and on scientific sensitivity studies performed during the OMI program, we expect that the retrievals of other trace gas molecules will also be possible with their required accuracies. The accuracies of the published absorption cross sections of the atmospheric constituents are significant contributors to the overall accuracies of the DOAS retrievals. This will include absolute accuracy as well as accurate spectral shapes and wavelength assignments. On the basis of these results we expect that the DOAS retrievals in flight will produce the anticipated accuracies. This will be verified in orbit for ozone, nitrogen dioxide, and the other target trace gases.

5. Conclusions

The spectral-slit-function calibration measurements, ozone and nitrogen dioxide absorption gas cell measurements, and zenith sky measurements performed with the Ozone Monitoring Instrument (OMI) that has flown on the EOS Aura satellite since 15 July 2004 have been presented and the results have been discussed. It is shown that the echelle optical stimulus allows for accurate calibration of the spectral slit functions as a function of wavelength and viewing direction with unprecedented accuracy for this type of instrument.

The *in situ* ozone and nitrogen dioxide absorption gas cell spectra demonstrate that convolution of accurate high-resolution absolute absorption cross-section spectra from the literature and accurately determined OMI spectral slit functions yields identical results, within the uncertainty margins, as absorption gas cell spectra directly measured with the OMI at flight-representative temperature and pressure conditions.

The results from the zenith sky measurements with the OMI flight instrument show that ozone and nitrogen dioxide can be retrieved from these spectra with the anticipated accuracies by use of a DOAS algorithm and that residual noise shows no observable instrument artifacts. The measured instrument performance, including the spectral stability and the signal-to-noise ratio, was as expected.

It has thus been demonstrated that the approach chosen for the OMI in which we use high-resolution absorption cross-section results from the literature convolved with accurately calibrated spectral slit functions for all wavelengths and viewing directions for the DOAS retrieval technique is valid for ozone and nitrogen dioxide, and thus presumably for other atmospheric molecules as well. Finally, it has been shown that the OMI is capable of making geophysical measurements of ozone and nitrogen dioxide from the ground with expected accuracies. Given the accuracies of the ground results, OMI is expected to meet its requirements of measuring the target Earth atmosphere trace gases and accomplish its mission instrument objectives.

This research was funded by the Netherlands Agency for Aerospace Programmes (M. Dobber, R. Dirksen, R. Voors, and P. Levelt) and the National Aeronautics and Space Administration (NASA) (G. H. Mount) within the framework of the Ozone Monitoring Instrument project. We thank Pepijn Veefkind (KNMI) for help with the DOAS retrievals.

References

1. R. D. McPeters, P. K. Bhartia, J. K. Arlin, J. R. Herman, C. G. Wellemeyer, C. J. Seftor, G. Jaross, O. Torres, L. Moy, G. Labow, W. Byerly, S. L. Taylor, T. Swissler, and R. P. Cebula, *Earth Probe Total Ozone Mapping Spectrometer* (TOMS) Data Products User's Guide, NASA Tech. Publ. 1998-206895 (NASA Goddard Space Flight Center, Greenbelt, Md., 1998).
2. U. Platt, "Differential optical absorption spectroscopy (DOAS)," in *Air Monitoring by Spectroscopic Techniques*, M. W. Sigrist, ed. (Wiley, New York, 1994).
3. J. M. C. Plane and N. Smith, "Atmospheric monitoring by differential optical absorption spectroscopy in environmental science," in *Advances in Spectroscopy*, R. J. H. Clark and R. E. Hester, eds. (Wiley, New York, 1994), Vol. 24.
4. F. W. P. Gotz, A. R. Meetham, and G. M. B. Dobson, "The vertical distribution of ozone in the atmosphere," Proc. R. Soc. London Ser. A **145,** 416–446 (1934).
5. C. L. Mateer and J. J. DeLuisi, "A new Umkehr inversion algorithm," J. Atmos. Terr. Phys. **54,** 537–556 (1992).
6. J. F. Grainger and J. Ring, "Anomalous Fraunhofer line profiles," Nature (London) **193,** 762–764 (1962).
7. J. Joiner and P. K. Bhartia, "The determination of cloud pressures from rotational Raman scattering in satellite backscatter ultraviolet measurements," J. Geophys. Res. **100,** 23019–23026 (1995).
8. R. L. Kurucz, I. Furenlid, J. Brault, and L. Testerman, "Solar flux atlas from 296 to 1300 nm," National Solar Observatory Atlas No. 1 (National Solar Observatory, Sunspot, N.M., 1984).
9. R. Dirksen, M. Dobber, P. Levelt, G. H. J. van den Oord, G. Jaross, M. Kowalewski, G. H. Mount, D. Heath, E. Hilsenrath, and J. de Vries, "The on-ground calibration of the ozone monitoring instrument from a scientific point of view," in *Sensors, Systems, and Next-Generation Satellites VII*, R. Meynart, S. P. Neeck, H. Shimoda, J. B. Lurie, and M. L. Aten, eds., Proc. SPIE **5234,** 400–410 (2003).
10. M. Dobber, R. Dirksen, P. F. Levelt, G. H. J. van den Oord, G. Jaross, M. Kowalewski, G. H. Mount, D. Heath, E. Hilsenrath, and R. Cebula, "Ozone Monitoring Instrument flight-model

on-ground and in-flight calibration," in *International Conference on Space Optics* (ICSO) ESA Pub. SP-554 (European Space Agency, Noordwijk, The Netherlands, 2004).
11. J. de Vries, G. H. J. van den Oord, E. Hilsenrath, M. te Plate, P. Levelt, and R. Dirksen, "Ozone Monitoring Instrument (OMI)," in *Imaging Spectrometry VII*, M. R. Descour and S. S. Chen, eds., Proc. SPIE **4480,** 315–325 (2001).
12. E. Laan, D. de Winter, J. de Vries, P. Levelt, G. H. J. van den Oord, A. Maelkki, G. Leppelmeier, and E. Hilsenrath, "Towards the use of the Ozone Monitoring Instrument (OMI)," in *Sensors, Systems, and Next-Generation Satellites V*, H. Fujisada, J. B. Lurie, and K. Weber, eds., Proc. SPIE **4540,** 270–277 (2001).
13. J. P. Burrows, A. Dehn, B. Deters, S. Himmelmann, A. Richter, S. Voigt, and J. Orphal, "Atmospheric remote-sensing reference data from GOME: 1. Temperature-dependent absorption cross sections of NO_2 in the 231–794 nm range," J. Quant. Spectrosc. Radiat. Transfer **60,** 1025–1031 (1998).
14. J. P. Burrows, A. Richter, A. Dehn, B. Deters, S. Himmelmann, S. Voigt, and J. Orphal, "Atmospheric remote-sensing reference data from GOME: 2. Temperature-dependent absorption cross sections of O_3 in the 231–794 nm range," J. Quant. Spectrosc. Radiat. Transfer **61,** 509–517 (1998).
15. K. Bogumil, J. Orphal, T. Homann, S. Voigt, P. Spietz, O. C. Fleischmann, A. Vogel, M. Hartmann, H. Bovensmann, J. Frerick, and J. P. Burrows, "Measurements of molecular absorption spectra with the SCIAMACHY proto-flight model: instrument characterisation and reference data for atmospheric remote-sensing in the 230–2380 nm region," J. Photochem. Photobiol. A **157,** 167–184 (2003).
16. J. W. Harder, J. W. Brault, P. V. Johnston, and G. H. Mount, "Temperature dependent NO_2 cross sections at high spectral resolution," J. Geophys. Res. **102,** 3861–3879 (1997).
17. S. R. Alliwell, M. van Roozendael, P. V. Johnston, A. Richter, and T. Wagner, "Analysis for BrO in zenith-sky spectra: an intercomparison exercise for analysis improvement," J. Geophys. Res. **107,** 4199–4218 (2002).
18. A. M. Bass and R. J. Paur, "The UV cross-sections of ozone: 1. Measurements in atmospheric ozone," in *Proceedings of the Quadrennial Ozone Symposium 1984* (Reidel, Dordrecht, The Netherlands, 1984), pp. 606–616.
19. J. B. Burrows, V. V. Rozanov, M. Vountas, A. Richter, U. Platt, H. Haug, L. Marquard, and K. Chance, "Study of the Ring Effect (final report)," prepared under ESA contract 10996/94/NL/CN (European Space Agency, Noordwijk, The Netherlands, 1996).
20. J. F. Noxon, "Nitrogen dioxide in the stratosphere and troposphere measured by ground-based absorption spectroscopy," Science **189,** 547–549 (1975).
21. J. F. Noxon, E. C. Whipple, and R. S. Hyde, "Stratospheric NO2: 1. Observational method and behavior at mid-latitude," J. Geophys. Res. **84,** 5047–5065 (1979).
22. J. F. Noxon, "Stratospheric NO2: 2. Global behavior," J. Geophys. Res. **84,** 5067–5076 (1979).
23. G. Mount, D. W. Rusch, J. F. Noxon, J. M. Zawodny, and C. A. Barth, "Measurements of stratospheric NO2 from the solar mesosphere explorer satellite. I. An overview of the results," J. Geophys. Res. **89,** 1327–1340 (1984).